Journal of Solid State Chemistry 182 (2009) 2560–2565

Contents lists available at ScienceDirect

Journal of Solid State Chemistry

journal homepage: www.elsevier.com/locate/jssc

Pulsed laser-induced oxygen deficiency at TiO_2 surface: Anomalous structure and electrical transport properties

Tomohiko Nakajima *, Tetsuo Tsuchiya, Toshiya Kumagai

National Institute of Advanced Industrial Science and Technology, Tsukuba Central 5, 1-1-1 Higashi, Tsukuba, Ibaraki 305-8565, Japan

ARTICLE INFO

Article history:
Received 3 June 2009
Received in revised form
26 June 2009
Accepted 4 July 2009
Available online 29 July 2009

Keywords:
Rutile $TiO_{2-\delta}$
Oxygen deficiency
Laser reduction
Metal–insulator transition
Stacking faults

ABSTRACT

We have studied pulsed laser-induced oxygen deficiencies at rutile TiO_2 surfaces. The crystal surface was successfully reduced by excimer laser irradiation, and an oxygen-deficient $TiO_{2-\delta}$ layer with 160 nm thickness was formed by means of ArF laser irradiation at 140 mJ/cm^2 for 2000 pulses. The $TiO_{2-\delta}$ layer fundamentally maintained a rutile structure, though this structure was distorted by many stacking faults caused by the large oxygen deficiency. The electrical resistivity of the obtained $TiO_{2-\delta}$ layer exhibited unconventional metallic behavior with hysteresis. A metal–insulator transition occurred at 42 K, and the electrical resistivity exceeded $10^4\,\Omega$ cm below 42 K. This metal–insulator transition could be caused by bipolaronic ordering derived from Ti–Ti pairings that formed along the stacking faults. The constant magnetization behavior observed below 42 K is consistent with the bipolaronic scenario that has been observed previously for Ti_4O_7. These peculiar electrical properties are strongly linked to the oxygen-deficient crystal structure, which contains many stacking faults formed by instantaneous heating during excimer laser irradiation.

1. Introduction

Titanium oxide materials are extremely popular owing to their many functions. In particular, photochemical reactions at TiO_2 surfaces have been well-studied [1]. Moreover, the introduction of 3*d* electrons to titanium oxides by means of oxygen defects produces various fascinating electronic and magnetic properties. For example, the ferromagnetism of TiO_2 with weak oxygen defects ($Ti^{3.9996+}$–$Ti^{3.80+}$) has been investigated [2–6]. In the Magnéli Ti_nO_{2n-1} phases, various electronic transport properties have been observed [7–10]. Ti_6O_{11} ($Ti^{3.67+}$) and Ti_5O_9 ($Ti^{3.60+}$) are polaronic insulators with a charge-ordering. With its increased oxygen deficiency (i.e., decreased *n*) relative to the aforementioned two titanium oxides, Ti_4O_7 ($Ti^{3.50+}$) is a paramagnetic metal with a metal–insulator transition corresponding to a bipolaronic ordering [7,9]. Thus, the physical properties of titanium oxides are significantly sensitive to oxygen deficiency. Oxygen-deficient $TiO_{2-\delta}$ has been prepared by various methods, including (1) a macroscopic heat treatment under low p_{O_2} or H_2 atmosphere [11], (2) a vapor process at low p_{O_2} [5], and (3) high-energy ion beam irradiation [6]. Of these three methods, we focused on the high-energy ion beam irradiation process, since the electronic states of local sites on crystal surfaces can be easily tuned by controlling the beam fluence. However, the detailed structural and physical properties of oxygen-deficient $TiO_{2-\delta}$ surfaces prepared by means of irradiation have not been investigated for a wide range of δ values.

In this work, we employed an excimer laser to prepare oxygen-deficient $TiO_{2-\delta}$ from rutile TiO_2. We have already reported that excimer laser irradiation at a high fluence (pulse duration: 26 ns) induces an oxygen deficiency at oxide surfaces, as observed in film-growth studies of an excimer laser assisted metal organic deposition [12–15]. In those studies, KrF laser irradiation at 100–140 mJ/cm^2 produced oxygen defects in thin films of perovskite oxides such as $CaTiO_3$ [14] and $Sm_{0.5}Ba_{0.5}MnO_3$ [15]. To further expand upon these oxygen deficiency studies, we studied oxygen deficiency in rutile TiO_2 surfaces prepared with ArF, KrF, and XeCl excimer lasers under a wide range of laser fluences, focusing on the variation of structural and electronic transport properties of the surfaces.

2. Experimental section

The TiO_2 crystals used for experiments were commercial single-crystal substrates of rutile TiO_2(100) (Shinkosha). The TiO_2 crystals were irradiated by ArF, KrF, and XeCl excimer lasers at room temperature in air. The pulse duration of these lasers is 25–30 ns. The structural properties of the obtained materials were examined by X-ray diffraction (Rigaku, SmartLab). The microscopic structures were probed at room temperature by means of cross-sectional transmission electron microscopy (TEM) and

* Corresponding author.
E-mail address: t-nakajima@aist.go.jp (T. Nakajima).

0022-4596/$ - see front matter © 2009 Elsevier Inc. All rights reserved.
doi:10.1016/j.jssc.2009.07.006

selected area electron diffraction (SAED) analysis with a JEM-2010 (JEOL) instrument operating at 200 kV. The variation in electrical resistance (R) under pulsed-laser irradiation was studied by a two-probe method. The electrical resistivity (ρ) curves as a function of temperature were measured by a four-probe technique. The temperature dependence of magnetization was studied by means of superconducting quantum interference device (SQUID) magnetometry at 1 T. The temperature variations during the laser irradiation process were calculated as functions of depth and time by the heat diffusion equation simplified into one-dimensional heat flow, as described in previous reports [16–18].

3. Results and discussion

3.1. Surface reduction of rutile TiO_2 and the peculiar structure

Fig. 1 shows the surface resistance of TiO_2 crystals as a function of pulse number under excimer laser irradiation. Under ArF laser irradiation, electrical conduction was observed at fluences above 60 mJ/cm^2, and the resistance decreased to approximately $3\times10^6\,\Omega$ after 2000 pulses (Fig. 1a). This conduction was caused by the reduction of Ti^{4+} to Ti^{3+} owing to an oxygen deficiency at the crystal surface. Such high-energy beam irradiation often produces oxygen defects, as reported previously [6,14,15]. The rate of decrease in resistance increased with increasing laser fluence, and the minimum resistance observed was $2\times10^4\,\Omega$ at 140 mJ/cm^2. This sample showed p-type conductivity at 300 K. Heavily oxygen-deficient $TiO_{2-\delta}$ is known to undergo a transition in conductivity from n-type to p-type when δ exceeds 0.333 [5,19,20]. Thus, the sample irradiated by the ArF laser at 140 mJ/cm^2 would have had a δ value near or exceeding these reported values. Under KrF and XeCl laser irradiation at different wavelengths, electrical conduction was observed at the TiO_2 surface for fluences above 80 mJ/cm^2; however, the minimum resistance in these cases reached only approximately $2\times10^5\,\Omega$ at 140 mJ/cm^2 (Fig. 1b and c). The difference in minimum resistance values between the cases of ArF, KrF, and XeCl laser irradiation is mainly due to the magnitude of the optical absorption coefficient for rutile TiO_2 at the wavelengths of each excimer laser. The optical absorption of TiO_2 at 193 nm (ArF) was larger than that of TiO_2 at 248 nm (KrF) and 308 nm (XeCl). In addition to the large absorption, the high photon energy of the ArF laser also contributed to the formation of oxygen deficiencies at the crystal surface, resulting in a favorable environment for the reduction of Ti^{4+} to Ti^{3+}. These results are supported by the observed pulse number dependence of the decreasing resistance (Fig. 1d). The resistance decrease observed for the TiO_2 surface under ArF laser irradiation was one order of magnitude faster than the decreases observed under KrF and XeCl laser irradiation.

Fig. 2 shows the $2\theta/\omega$ scans of X-ray diffraction for the unirradiated rutile TiO_2(100) substrate and for TiO_2(100) after ArF laser irradiation at 140 mJ/cm^2 for 2000 pulses. The 200 and 400 diffraction peaks from Cu$K\alpha$- and Cu$K\beta$-lines were clearly observed in the pattern of the unirradiated TiO_2(100) substrate. However, a new diffraction peak at 19.38° indexed to the 100 reflection in the tetragonal unit cell appeared after laser irradiation. The 100 reflection is prohibited by the extinction rule in the space group $P4_2/mnm$ for the rutile TiO_2 structure [21]. Therefore, the emergence of the 100 peak in the irradiated sample indicates lowered symmetry due to the structural distortion derived from the oxygen deficiency near the crystal surface. After the laser irradiation, the fundamental 200 and 400 peaks derived from the TiO_2(100) substrate were shifted to higher diffraction angles, and new diffraction peaks appeared near the fundamental peaks at lower angles (Fig. 2, insets). The appearance of these

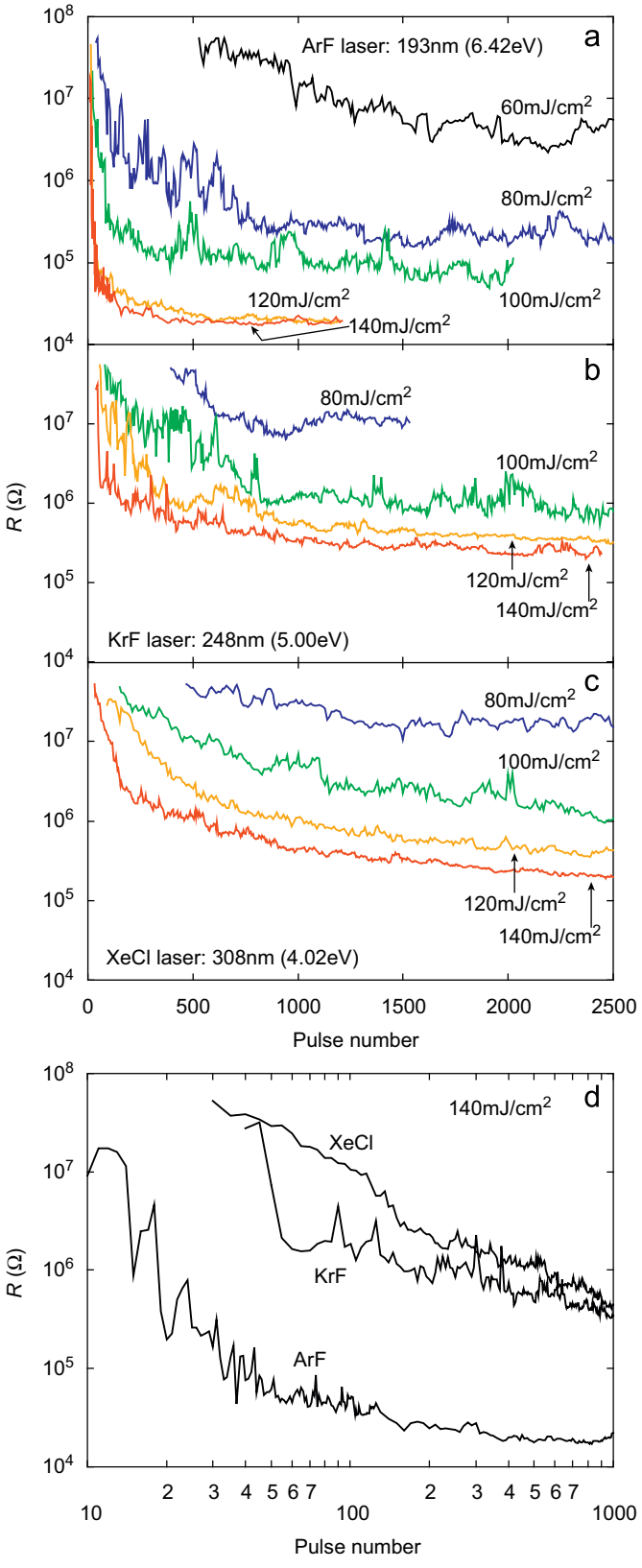

Fig. 1. Surface resistance of TiO_2(100) substrates as a function of pulse number irradiated by (a) ArF, (b) KrF, (c) XeCl lasers, and (d) enlarged plot of pulse number dependence for the surface resistance of TiO_2(100) substrates irradiated by ArF, KrF, and XeCl lasers at 140 mJ/cm^2.

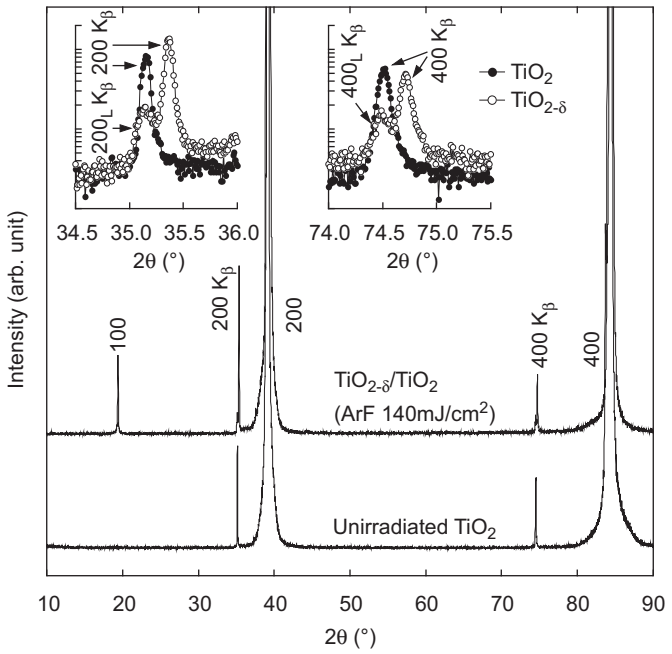

Fig. 2. $2\theta/\omega$ X-ray diffraction patterns for an unirradiated rutile $TiO_2(100)$ substrate and for $TiO_2(100)$ after ArF laser irradiation at 140 mJ/cm^2 for 2000 pulses. The subscript L represents the oxygen-deficient layer.

peaks suggests that an oxygen-deficient $TiO_{2-\delta}$ with different lattice parameters was formed as a new layer on the rutile $TiO_2(100)$ substrate by the laser irradiation. The *d*-spacing of the *a*-axis for the emergent new layer was 0.6% longer than that of the base crystal.

Fig. 3a shows a cross-sectional TEM image obtained along the [001] zone axis for the sample after ArF laser irradiation at 140 mJ/cm^2. In the TEM image, a phase separation was clearly confirmed near the crystal surface at 160 nm depth, indicating the presence of the oxygen-deficient $TiO_{2-\delta}$ layer on the $TiO_2(100)$ substrate. The presence of this layer was also confirmed by X-ray diffraction analysis, as mentioned above. The phase separation derived from the presence of the $TiO_{2-\delta}$ layer indicates that the oxygen deficiencies did not occur gradually but was homogeneous to some extent in the surface layer. In the SAED pattern of the $TiO_{2-\delta}$ layer, streaks were observed along the [100] direction, and the angle (γ) between the *a*- and *b*-axes was 90.44° (Fig. 3b), indicating that the laser irradiation decreased the structural symmetry of the $TiO_{2-\delta}$ layer to monoclinic or triclinic. At the lower part of the interface between the $TiO_{2-\delta}$ layer and the $TiO_2(100)$ substrate, the γ value decreased to 90.26°, and weak satellite spots were observed along the [100] direction (Fig. 3c). These satellite spots almost disappeared at around 400 nm depth, and the γ value decreased to 90.05° (Fig. 3d). This means that structural distortion also occurred in the lower region of the substrate, and the structural symmetry decreased from tetragonal to monoclinic or triclinic as was observed for the upper $TiO_{2-\delta}$ layer. The 100 peak observed in the X-ray diffraction pattern must be derived from this structural distortion. In addition, the *d*-spacing of *a*-axis at around 400 nm depth was approximately 0.9% shorter than that of the $TiO_{2-\delta}$ layer evaluated from the SAED patterns. This result also supports the X-ray diffraction analysis. Fig. 3e shows a high-resolution TEM image of the $TiO_{2-\delta}$ layer along the [001] zone axis. Many stacking faults are observed along the [010] direction in this image. These many stacking faults could be due to the large oxygen deficiency in the $TiO_{2-\delta}$ layer, thus causing a decrease in symmetry as well as the streak reflections

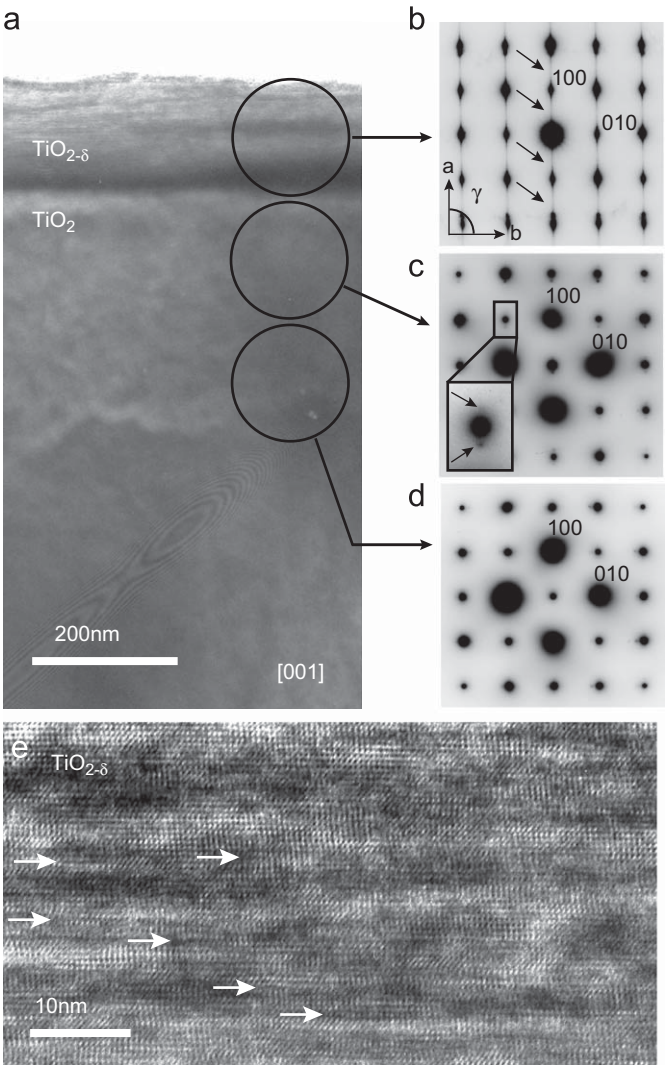

Fig. 3. (a) Cross-sectional TEM image obtained along the [001] zone axis for a $TiO_2(100)$ substrate irradiated by an ArF laser at 140 mJ/cm^2. (b)–(d) SAED patterns observed at the circled regions in the TEM image. (e) High-resolution TEM image along the [001] zone axis of the $TiO_{2-\delta}$ layer. The white arrows indicate stacking faults in the structure.

observed in the SAED pattern. However, it is noteworthy that the fundamental structure of $TiO_{2-\delta}$ layer remained rutile, even though the symmetry was lowered by the presence of many stacking faults.

The reciprocal space mappings around the (220) reflection for the unirradiated $TiO_2(100)$ substrate and for the sample irradiated by the ArF laser at 140 mJ/cm^2 are shown in Fig. 4. The observed strong (220) reflection, large crystal truncation rod scattering, and narrow peak width of the Q_x profile at the (220) reflection indicate that the unirradiated $TiO_2(100)$ substrate was highly crystalline (Fig. 4a). In contrast, significant diffuse scattering was clearly observed around the (220) reflection for a wide range of Q_x (−0.04–0.04) in the irradiated sample (Fig. 4b), indicating a strong local lattice distortion near the surface of the sample. The observed large crystal truncation rod scattering parallel to the surface normal vector ($Q_x = 0$) of the irradiated sample suggests that $TiO_{2-\delta}$ was homogeneously formed at the crystal surface.

Though the Magnéli phase Ti_nO_{2n-1} ideally appears as a second phase when the oxygen vacancy of $TiO_{2-\delta}$ increases to $\delta = 0.01$ by means of normal macroscopic heating in H_2 flow [11], the Magnéli phase was not formed at all in the samples processed by

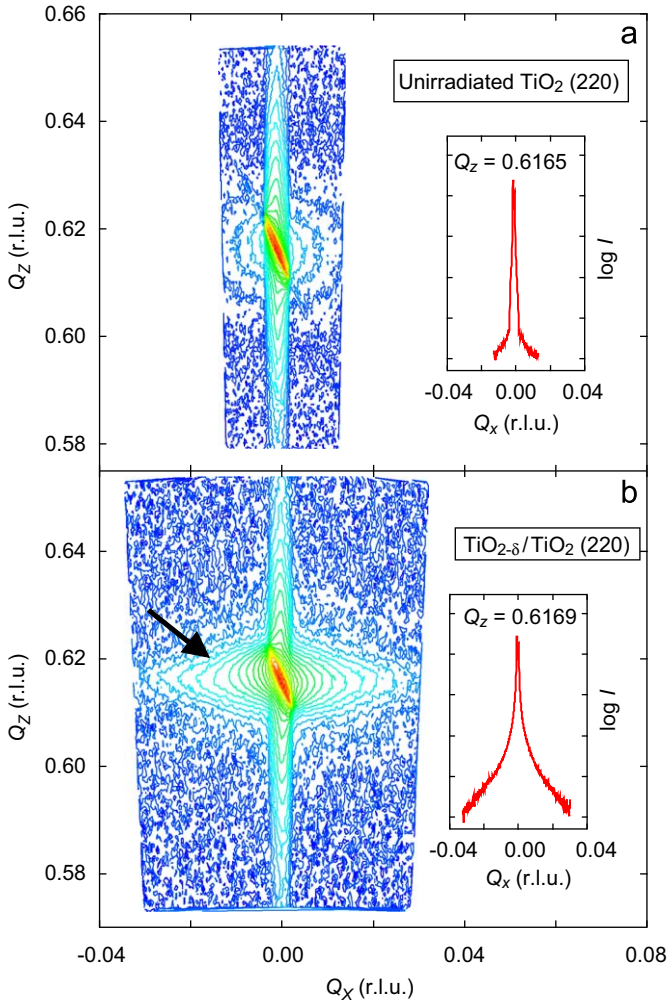

Fig. 4. Reciprocal space mappings around the (220) reflection for the (a) unirradiated TiO_2(100) substrate and (b) laser-irradiated $TiO_{2-\delta}/TiO_2$(100). The insets show the Q_x profiles at the (220) reflection.

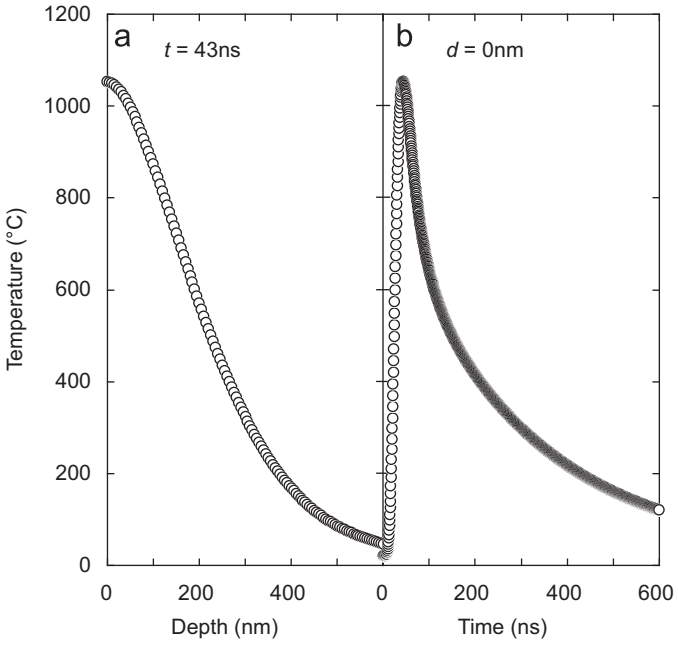

Fig. 5. Numerical simulations for (a) depth and (b) time dependence of the temperature variation for a TiO_2 substrate subjected to ArF laser irradiation at a fluence of 140 mJ/cm^2. The initial substrate temperature was fixed at 20 °C.

pulsed-laser irradiation. Fig. 5 shows simulated surface temperature profiles as functions of depth and time for the sample irradiated by the ArF laser at 140 mJ/cm^2. The sample temperatures at 0 and 160 nm depths were photo-thermally heated to 1050 and 690 °C, respectively (Fig. 5a). However, the sample was heated to high temperatures instantaneously, e.g., the sample was at 700 °C for only ~60 ns. Therefore, we concluded that the oxygen release reaction occurred on the order of nanoseconds, and then it would realize to grab the thermal nonequilibrated phase. These results suggest that the nanoseconds-long temperature elevation and quenching enabled the $TiO_{2-\delta}$ layer to maintain a rutile structure, even though a large number of oxygen defects were produced near the surface. This retained original structure is a feature unique to pulsed-laser reduction processing and has great potential for applications in fabrication of thin-film materials with a thermal nonequilibrated crystal structure.

3.2. Anomalous electrical transport properties of $TiO_{2-\delta}$

Fig. 6 shows the electrical resistivity (ρ) of samples irradiated by the ArF laser for 2000 pulses (the ρ values were calculated for a film thickness of 160 nm). The sample irradiated at 60 mJ/cm^2 exhibited semiconductive behavior, but this sample did not show a normal Arrhenius-like temperature variation, and the increment of ρ at low temperature was not large. This resistivity behavior could be due to a modulation of the magnitude of reduction along the depth direction in this sample, although exact estimation of this modulation is difficult. Thus, the net conductivity observed probably represented the average of both highly reduced (high conductivity) and minimally reduced (low conductivity) parts within the sample. The $TiO_{2-\delta}$ sample prepared at 80 mJ/cm^2 was not a semiconductor. Its ρ values varied minimally down to 80 K, and a transition to an insulator was observed at 70 K. The sample irradiated at 100 mJ/cm^2 showed weak metallic behavior below 100 K, and a metal–insulator (MI) transition occurred at 50 K. This metallic behavior was dramatically enhanced when the samples were irradiated above 120 mJ/cm^2. Finally, the $TiO_{2-\delta}$ layer prepared at 140 mJ/cm^2 showed a semiconductor–metal transition at 300 K. The ρ values for this sample exhibited a large decrease below 300 K, and ρ reached $4.5\times10^{-2}\,\Omega$ cm at 42 K. For this sample, ρ anomalously changed with a larger decrease rate than that observed for T-linear behavior down to 42 K ($d^2\rho/dT^2<0$) (Fig. 6b). In the Magnéli Ti_nO_{2n-1} phase, Ti_5O_9 and Ti_6O_{11} show polaronic behavior at temperatures above the transition to a charge-ordered insulator phase [9,22]. In Ti_4O_7 above the MI transition temperature, ρ is well defined as a normal metal [8,9]. Furthermore, the metallic behavior as observed in the present laser-irradiated samples has never been reported for $TiO_{2-\delta}$ samples with higher δ values [23]. In addition to this peculiar metallic behavior, we also observed hysteresis ($\Delta T = 14$ K) over a wide range of temperatures (50–250 K). This hysteresis was reproducible; therefore, we concluded that it was caused by the irreversible formation or disappearance of stacking faults rather than by an intrinsic structural change. This observed behavior indicates that there are two temperature-dependent phases in the metallic state, although the transition from the high-temperature phase (M1) to the low-temperature phase (M2) appeared to occur slowly as a first-order transition with latent heat. Thus, the anomalous metallic behavior observed here could be explained as

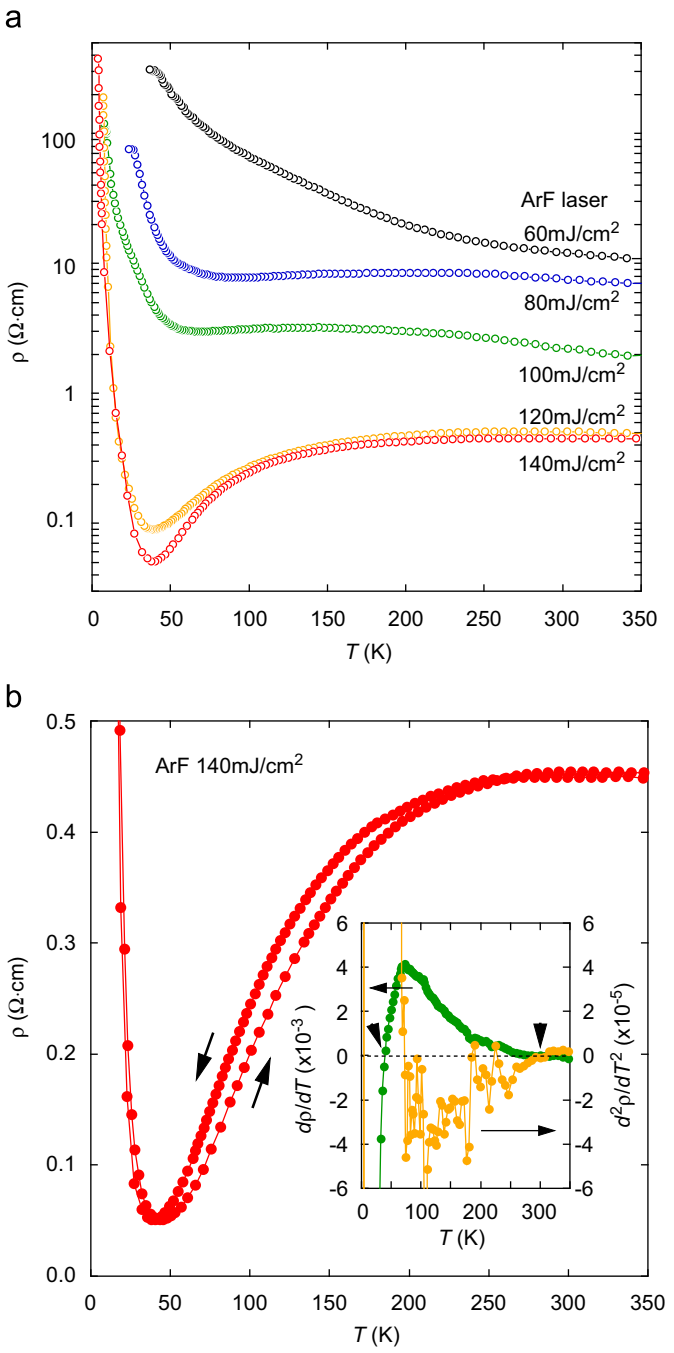

Fig. 6. (a) Temperature dependence of resistivity for $TiO_{2-\delta}$ prepared by ArF laser irradiation at 60–140 mJ/cm^2. All resistivity data were calculated for an oxygen-deficient layer with a thickness of 160 nm. (b) Temperature dependence of resistivity during heating and cooling for $TiO_{2-\delta}$ prepared by ArF laser irradiation at 140 mJ/cm^2. The inset shows the first- and second-order differentials of ρ.

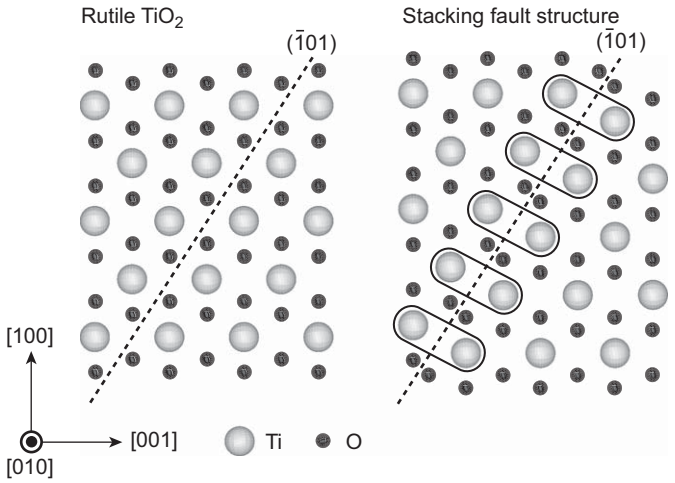

Fig. 7. Schematic illustrations of rutile TiO_2 and its stacking fault structures projected along the [010] zone axis.

a gradual phase transition from M1 with low conductivity to M2 with high metallicity. In other words, this slow transition can be regarded as a kind of relaxor behavior [24,25] caused by the phase separation between the original rutile blocks and inhomogeneously distributed stacking faults.

At 42 K, the MI transition occurred, and ρ exceeded 5.0×10^2 Ω cm. However, this transition had no hysteresis, although a huge resistivity change ($\Delta\rho > 10^4$ Ω cm) was observed. Here, we focused on the MI transition in Ti_4O_7: the Ti–Ti distance is shortened below a structural transition in Ti_4O_7, and then a bipolaronic charge-ordering occurs owing to the Ti^{3+}–Ti^{3+} and Ti^{4+}–Ti^{4+} pairings [8]. In our study, we have already mentioned that many stacking faults were observed in the rutile structure of the laser-irradiated $TiO_{2-\delta}$ layer. The presence of stacking faults has also been reported in rutile TiO_2. For example, a stacking fault structure in the (1̄01) plane is well known [26]. The stacking fault in the (1̄01) plane in the rutile structure results in a shorter Ti–Ti bond length compared to that of the original structure, as shown in Fig. 7. This indicates that the crystal structure of the laser-irradiated $TiO_{2-\delta}$ layer might have contained Ti–Ti pairings if stacking faults of this type were formed. If Ti^{4+} and Ti^{3+} ions are assumed to coexist along many stacking faults in the rutile structure, then the origin of the MI transition in the laser-irradiated $TiO_{2-\delta}$ can be also explained by bipolaronic charge-ordering, as is observed for Ti_4O_7. Fig. 8a shows the magnetization (M) curve of a $TiO_{2-\delta}$ layer. This M curve was obtained by subtracting M values for the unirradiated TiO_2 from those obtained for the laser-irradiated $TiO_{2-\delta}/TiO_2$. The temperature dependence of M exhibited neither long-range ferromagnetic ordering nor Curie–Weiss paramagnetic behavior at low temperature. M increased slightly at around 220 K, decreased at temperatures lower than 60 K, and was nearly constant below 50 K. We concluded that the origin of this M behavior consisted of two phases, P1 and P2. The P1 phase corresponded to the oxygen-deficient rutile blocks in the structure, which have a ferromagnetic transition as reported previously [2–6]. However, the ferromagnetic transition temperature was lowered, and its moment was very weak. Because the ferromagnetic correlation was significantly short-ranged owing to the presence of discrete rutile units separated by many stacking faults. The P2 phase corresponded to the regions near the stacking faults. If bipolaronic ordering occurred along the stacking faults, then M should show a temperature-independent behavior below 42 K since the spins of the Ti–Ti pair have a singlet ground state [8,10]. The observed constant value of M below 50 K strongly supports this bipolaronic scenario in the $TiO_{2-\delta}$ layer. A schematic magnetization behavior in which the M of P1 is added to that of P2 well expresses the experimental data (Fig. 8b).

Therefore, the anomalous electrical conductivity in the laser-irradiated $TiO_{2-\delta}$ is very interesting because of the link between this behavior and the peculiar crystal structure of this phase, which is induced by a nanosecond-long oxygen release reaction during pulsed-laser irradiation. The inhomogeneously distributed interstitials may not have induced superconductivity beyond the MI transition under high pressure that is expected for Ti_4O_7

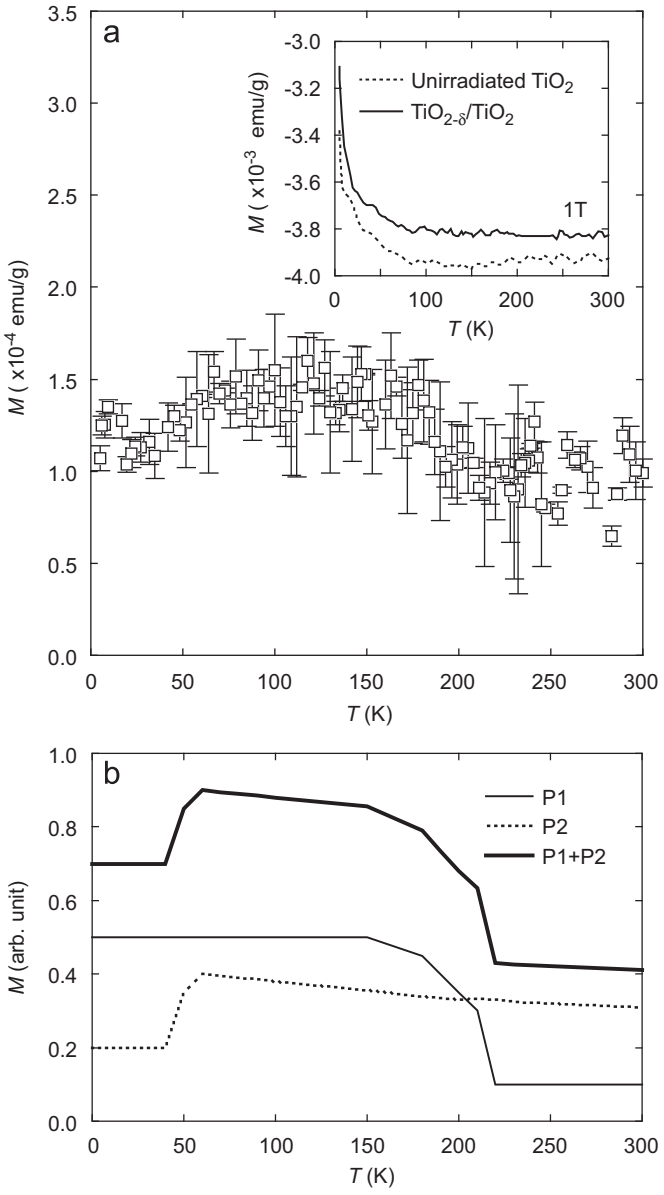

Fig. 8. (a) Magnetization of a 160-nm thick $TiO_{2-\delta}$ layer as a function of temperature. The inset shows the magnetization for unirradiated and laser-irradiated TiO_2. (b) Schematic magnetization behaviors for two phases in the $TiO_{2-\delta}$ layer. The P1 phase corresponds to the rutile blocks with ferromagnetic correlation, and the P2 phase corresponds to the region near the stacking faults with Ti–Ti pairings. The steep drop in the P2 magnetization curve was caused by bipolaronic ordering.

[10,27] because of a desired structural coherency. On the contrary, we believe that the artificially induced relaxor behavior caused by laser irradiation is very promising for ferroelectric and magnetic applications.

4. Conclusions

We have studied pulsed-laser-induced oxygen deficiencies at rutile TiO_2 surfaces. An oxygen-deficient $TiO_{2-\delta}$ layer with 160 nm thickness was formed by means of ArF laser irradiation at 140 mJ/cm^2 for 2000 pulses. The $TiO_{2-\delta}$ layer fundamentally maintained a rutile structure, though this structure was distorted by many stacking faults caused by the large oxygen deficiency, which in turn lowered the structural symmetry from tetragonal to monoclinic or triclinic. The electrical resistivity of the obtained $TiO_{2-\delta}$ layer was metallic at 42–300 K and exhibited hysteresis over a wide range of temperatures, consistent with relaxor-like behavior. This unconventional metallic behavior must have originated from the short-range structural coherency caused by inhomogeneously dispersed interstitials. An MI transition occurred at 42 K, and the electrical resistivity exceeded $10^4\,\Omega$ cm below 42 K. This MI transition could be caused by bipolaronic ordering derived from Ti–Ti pairings that formed along the stacking faults. The constant magnetization behavior observed below 42 K is consistent with the bipolaronic scenario that has been observed previously for Ti_4O_7. These peculiar electrical properties are strongly linked to the oxygen-deficient crystal structure, which contains many stacking faults formed by instantaneous heating during excimer laser irradiation.

Acknowledgments

We are grateful to Y. Ueda and H. Ueda at the Institute for Solid State Physics, University of Tokyo, for valuable discussions. The TEM observations, electrical resistivity measurements, and magnetization measurements were carried out using the facilities of the Materials Design and Characterization Laboratory, Institute for Solid State Physics, University of Tokyo.

References

[1] A. Fujishima, K. Honda, Nature 238 (1972) 37.
[2] J.M.D. Coey, M. Venkatesan, P. Stamenov, C.B. Fitzgerald, L.S. Dorneles, Phys. Rev. B 72 (2005) 024450.
[3] N.H. Hong, J. Sakai, N. Poirot, V. Brizé, Phys. Rev. B 73 (2006) 132404.
[4] S.D. Yoon, Y. Chen, A. Yang, T.L. Goodrich, X. Zuo, D.A. Arena, K. Ziemer, C. Vittoria, V.G. Harris, J. Phys. Condens. Matter 18 (2006) L355.
[5] S.D. Yoon, V.G. Harris, C. Vittoria, A. Widom, J. Phys. Condens. Matter 19 (2007) 326202.
[6] S. Zhou, E. Čižmár, K. Potzger, M. Krause, G. Talut, M. Helm, J. Fassbender, S.A. Zvyagin, Phys. Rev. B 79 (2009) 113201.
[7] D. Alder, Solid State Phys. 21 (1968) 1.
[8] M. Marezio, D.B. McWhan, P.D. Dernier, J.P. Remeika, J. Solid State Chem. 14 (1976) 1429.
[9] H. Ueda, K. Kitazawa, H. Takagi, T. Matsumoto, J. Phys. Soc. Jpn. 71 (2002) 1506.
[10] C. Acha, M. Monteverde, M. Núnez-Regueiro, A. Kuhn, M.A. Alario Franco, Eur. Phys. J. B 34 (2003) 421.
[11] M. Radecka, A. Trenczek-Zajac, K. Zakrzewska, M. Rekas, J. Power Sources 173 (2007) 816.
[12] T. Tsuchiya, A. Watanabe, Y. Imai, H. Niino, I. Yamaguchi, T. Manabe, T. Kumagai, S. Mizuta, Jpn. J. Appl. Phys. 38 (1999) L823.
[13] T. Tsuchiya, T. Yoshitake, Y. Shimakawa, I. Yamaguchi, T. Manabe, T. Kumagai, Y. Kubo, S. Mizuta, Jpn. J. Appl. Phys. 42 (2003) L956.
[14] T. Nakajima, T. Tsuchiya, T. Kumagai, Jpn. J. Appl. Phys. 46 (2007) L365.
[15] T. Nakajima, T. Tsuchiya, K. Daoudi, M. Ichihara, Y. Ueda, T. Kumagai, Chem. Mater. 19 (2007) 5355.
[16] D. Bäuerle, Laser Processing and Chemistry, Springer, Berlin, Heidelberg, New York, 2000.
[17] T. Nakajima, T. Tsuchiya, M. Ichihara, H. Nagai, T. Kumagai, Chem. Mater. 20 (2008) 7344.
[18] T. Nakajima, T. Tsuchiya, M. Ichihara, H. Nagai, T. Kumagai, Appl. Phys. Express 2 (2009) 023001.
[19] Q. He, Q. Hao, G. Chen, B. Poudel, X. Wang, D. Wang, Z. Ren, Appl. Phys. Lett. 91 (2007) 052505.
[20] N. Okinaka, T. Akiyama, Jpn. J. Appl. Phys. 45 (2006) 7009.
[21] S.C. Abrahams, J.L. Bernstein, J. Chem. Phys. 55 (1971) 3206.
[22] M. Marezio, D. Tranqui, S. Lakkis, C. Schelenker, Phys. Rev. B 16 (1977) 2811.
[23] D.S. McLachlan, Phys. Rev. B 25 (1982) 2285.
[24] I.W. Chen, P. Li, Y. Wang, J. Phys. Chem. Solids 57 (1996) 1525.
[25] T. Kimura, Y. Tokura, R. Kumai, Y. Okimoto, Y. Tomioka, J. Appl. Phys. 89 (2001) 6857.
[26] S. Yamada, M. Tanaka, J. Electron Microsc. 1 (1997) 67.
[27] M. Marezio, A. Gauzzi, F. Licci, E. Gilioli, Physica C 338 (2000) 1.